catalysts

MDPI

Review

The Influence of Photocatalytic Reactors Design and Operating Parameters on the Wastewater Organic Pollutants Removal—A Mini-Review

Alexandru Enesca

Product Design, Mechatronics and Environmental Department, Transilvania University of Brasov, Eroilor 29 Street, 35000 Brasov, Romania; aenesca@unitbv.ro

Abstract: The organic pollutants removal by conventional methods (adsorption, coagulation, filtration, microorganism and enzymes) showed important limitation due to the reluctance of these molecules. An alternative to this issue is represented by the photocatalytic technology considered as an advanced oxidation process (AOP). The photoreactors design and concepts vary based on the working regime (static or dynamic), photocatalyst morphology (powders or bulk) and volume. This mini-review aims to provide specific guidelines on the correlations between the photoreactor concept characteristics (working regime, volume and flow rate), irradiation scenarios (light spectra, irradiation period and intensity) and the photocatalytic process parameters (photocatalyst materials and dosage, pollutant type and concentration, pollutant removal efficiency and constant rate). The paper considers two main photoreactor geometries (cylindrical and rectangular) and analyses the influence of parameters optimization on the overall photocatalytic efficiency. Based on the systematic evaluation of the input data reported in the scientific papers, several perspectives regarding the photocatalytic reactors' optimization were included.

Keywords: reactors; flow rate; photocatalysts; light radiation; organic pollutants

Citation: Enesca, A. The Influence of Photocatalytic Reactors Design and Operating Parameters on the Wastewater Organic Pollutants Removal—A Mini-Review. *Catalysts* **2021**, *11*, 556. https://doi.org/10.3390/catal11050556

Academic Editor: Aida M. Diez

Received: 7 April 2021
Accepted: 26 April 2021
Published: 27 April 2021

1. Introduction

Water represents a vital element for all living organisms and preserving it in a free pollutant state is essential [1]. Due to the high increase of the population, most of them living in the urban area have accelerated the pressure on the treatment water plant to provide fresh and safe water. In the same time the wastewater plants encounter significant difficulties to address the increase of contaminants concentration and structure [2–4]. Among these contaminants, the organic pollutants such as phenols [5], pesticides [6], pharmaceutical [7] and dyes [8] raise special issues due to their impact on human health and aquatic life. The organic pollutants removal by conventional methods (adsorption, coagulation, filtration, microorganism and enzymes) showed important limitation due to the reluctance of these molecules [9,10]. One disadvantage of the traditional wastewater treatments is given by the incomplete mineralization of the organic pollutant, which may result in the formation of other organic molecules with high toxicity potential [11,12]. Additionally, the conventional methods have failed in removing highly toxic pollutants found most often in low or even trace concentrations. These pollutants originating from medical care or industrial activities may persist for long periods of time into the contaminated environment [13]. Addressing these issues in a sustainable manner require an integrated procedure that includes economic and political factors. An alternative to this issue is represented by the photocatalytic technology considered as an advanced oxidation process (AOP) [14].

The driving force of the photocatalytic process is the light irradiation, able to provide enough energy necessary to produce oxidative species involved in organic pollutant mineralization. Sun is a continuous source of energy sending around 5×10^{22} J each year on the Earth

surface [15]. There are several approaches (photobiological, photothermal, photovoltaic and photochemical) aiming to convert the photon energy into an available energy form [16–18].

Besides the irradiation source, photocatalyst material and the photoreactors structure play an important role on the photocatalytic performance evaluated based on the pollutant removal efficiency. The additional components such as pumps, valves, pipes and the working regime (static or dynamic) contribute to the overall characteristics of the photocatalytic process [19,20]. Keeping high standards in wastewater treatment procedures require finding a suitable balance between the technological parameters, chemical substances consumption and economical costs [21,22]. The photocatalytic processes can be used for the indoor air decontamination as well. Obviously, the photoreactors must be adapted to include the air-proof concept and gas flow dynamic, which are mandatory during the design step. Adapting photocatalytic technologies to the conventional wastewater plant is a key factor to be considered for large scale applications. Both material and process optimizations are required in order to improve the pollutant addressability and the overall photocatalytic efficiency. For example, doping photocatalytic materials can significantly increase the charge carrier's concentration due to the use of larger light absorption spectra. Coupling semiconductors with other materials (metals, wood, fly ash, etc.) can tune properties such as: conductivity, surface energy, porosity or crystallinity. Finding new pathways that combine the advantages of simple technology, energy sustainability and environmentally friendly materials is a prerequisite for future applications.

This mini-review aims to provide specific guidelines on photoreactors design and parameters optimization for wastewater treatment, based on representative achievement published by researchers. Due to the length limitation of the mini-review, there may be others representative papers that are not included here. The paper considers two main photoreactor geometries (cylindrical and rectangular) and analyzes the correspondence between the photoreactor concept characteristics (working regime, volume and flow rate), irradiation scenarios (light spectra, irradiation period and intensity) and the photocatalytic process parameters (photocatalyst materials and dosage, pollutant type and concentration, pollutant removal efficiency and constant rate). The geometrical shape is considered one of the main factors that may influence the photocatalytic activity. Based on the reactor design, the photons conversion or photocatalyst diffusion may be optimizing in order to enhance the pollutant removal. The paper shows that reactors with similar shape exhibit various photocatalytic efficiency, function of the working parameters. Based on the systematic evaluation of the input data reported in the scientific papers, several perspectives regarding the photocatalytic reactors' optimization were included.

2. Photocatalytic Reactors for Wastewater Treatment: Working Principles and Components

The advanced oxidation processes for wastewater treatment can be divided in two main groups: homogeneous and heterogeneous light induced technologies. Homogenous technologies include ozonation (UV/O_3 and $UV/O_3/H_2O_2$) and photo-Fenton ($UV/Fe^{2+}/H_2O_2$) processes [23–25]. Considering as an example, the photo-Fenton process, the oxidative species (hydroxide radicals ·OH) are generated from H_2O_2 photolysis mediated by UV reduction of Fe^{3+} ions into Fe^{2+} (Equations (1) and (2)). The ·OH photogeneration require a maximum pH around 3, which is the precondition for Fe^{+3} ions to exist as $Fe(OH)^{2+}$ [26–28].

$$H_2O_2 + h\nu(UV) \rightarrow 2 \cdot OH \quad (1)$$

$$Fe^{3+} + h\nu(UV) + H_2O \rightarrow Fe^{2+} + H^+ + \cdot OH \quad (2)$$

The homogenous photocatalysis can be designed to ensure homogenous reagents mixing and at the same time to provide the optimum light intensity distribution. The process can be optimized based on several parameters such as: pH of the solution, iron salt and H_2O_2 dosage, mixing rate or temperature. An important disadvantage of homogeneous photocatalysis is represented by the pH limitations and high chemical substances consumption [29–31].

An alternative is represented by the heterogeneous photocatalysis, which typically use solid catalysts (semiconductors) to remove the organic pollutants under irradiation due to the reduction and oxidation (redox) reactions induced by the photogenerated charge carriers. If the chemical potential of the photoinduced electrons from the conduction-band (CB) is lower than + 0.5 V versus the normal hydrogen electrode (NHE), they are considered as reductants with strong oxidizability [32–34]. Accordingly with Figure 1 the photocatalytic process includes: (i) charge carriers pairs generation under irradiation, (ii) the migration of photogenerated charge carriers on the catalyst surface and (iii) the redox reaction initiated by the oxidative (·OH) and superoxide ($\cdot O_2^-$) radicals (Equations (3) and (4)). Direct oxidation of the organic molecules by photogenerated holes can occur. The subsequent reactions between $\cdot O_2^-$ with H^+ can produce hydroperoxyl radicals (·OOH) and H_2O_2 (Equations (5)–(7)). The heterogenous photocatalytic process aims to induce organic pollutant mineralization (CO_2 and H_2O). However, based on the process efficiency, pollutant composition and structure, the formation of additional products (e.g., salts and acids) is possible (Equation (8)) [35–37].

$$H_2O + h_{VB}^+ \rightarrow \cdot OH + H^+ \quad (3)$$

$$O_2 + e_{CB}^- \rightarrow \cdot O_2^- \quad (4)$$

$$O_2^- + H^+ \rightarrow \cdot OOH \quad (5)$$

$$OOH + \cdot OOH \rightarrow H_2O_2 + O_2 \quad (6)$$

$$H_2O_2 + e_{CB}^- \rightarrow \cdot OH + HO^- \quad (7)$$

$$\text{Poll tan t} + \cdot OH + \cdot O_2^- \rightarrow CO_2 + H_2O + \text{Bi} - \text{products} \quad (8)$$

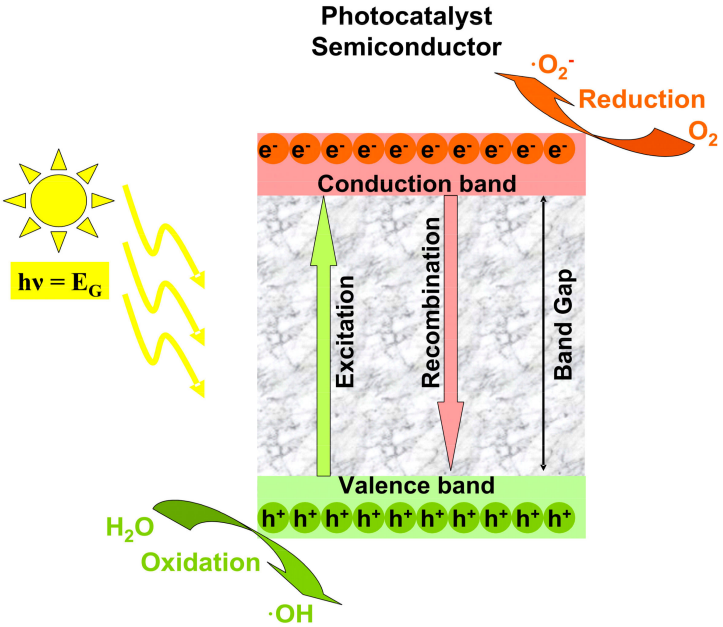

Figure 1. Mechanism of oxidative radical's development.

Figure 2 presents the main components of the photoreactor set-up technology: photocatalyst, light irradiations, auxiliaries, additives, etc. There are two major properties to be considered regarding the semiconductors photocatalysts: (1) composition and (2) morphology. The composition plays an important role in the charge carrier's mobility during the photocatalytic activity [38,39]. The basic composition includes a mono-component photocatalyst such as TiO_2 [40], WO_3 [41], ZnO [42], Cu_2S [43], etc. Even optimized by doping or surface photosensitization, these materials exhibit disadvantages related to charge recombination, limited absorption range and low chemical stability [44–46]. The multi-component

photocatalyst, called heterostructures, benefit from the extended light spectra being able to use UV, visible or near infra-red photoexcitation depending on their energy band gaps values and ability to produce oxidative radicals involved in organic pollutants removal. The heterostructure can follow several mechanisms: type I junctions [47], type II junctions [48], Schottky junctions [49], Z-scheme mechanism [50] or S-scheme mechanisms [51]. These heterostructures contain at least two semiconductors with suitable position of energy bands, excepting Schottky junction, which may include one semiconductor coupled with a metal. Owing to the versatile band energy structures and efficient charge carrier's separation, the heterostructured photocatalyst are characterized by a superior performance comparing to their individual constituents.

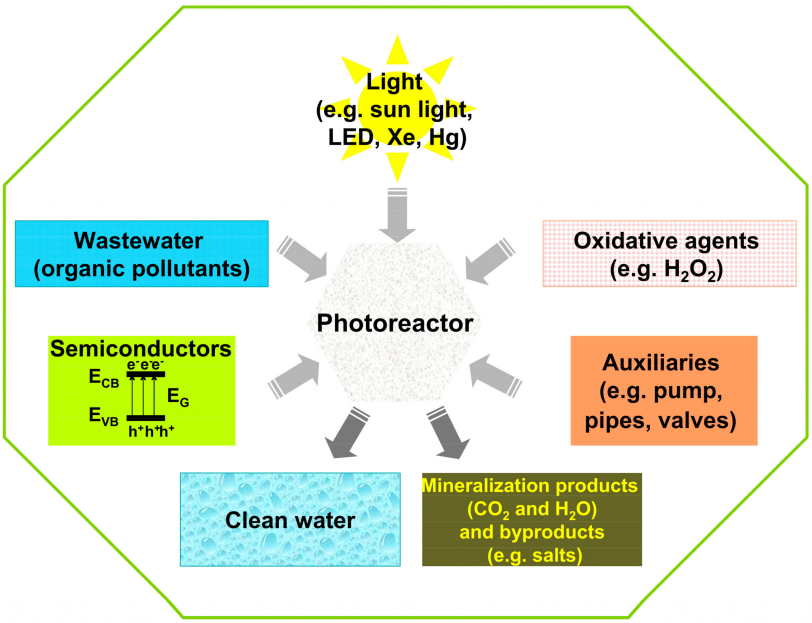

Figure 2. Components of the photoreactor set-up.

Photocatalysts morphology is a key parameter considering that photocatalysis is a surface dependent process. Nanoparticle semiconductors and immobilized thin films are prevalent in the papers reporting the photoreactors development. Increasing the active surface area is a prerequisite for good photocatalytic efficiency allowing the formation of high energy active sites participating in the oxidative radical's development [52,53]. The flower like and sheets morphologies were predominant in the heterostructure photocatalyst, due to their ability to include a larger number of surface active sites and to promote high photocatalytic activity [54]. Tailoring the photocatalyst morphology is an attribute of the preparation procedure, chemical composition and technical parameters.

The light source is an important parameter to be considered when designing the photoreactor. The light intensity, spectral range and radiation source position in the photocatalytic set-up have a significant influence on the overall pollutant removal efficiency [55,56]. Excepting the case when the sunlight is directly use for photocatalyst excitation, all the artificial light sources must be configured based on uniform photons distribution and process energy sustainability. The intensity of the light source must consider the penetration index required to overcome the scattering induced by the working environment. Additionally, the spectral range of the light sources should be correlated with the photocatalyst characteristics required to overcome the band gap energy [57–59].

The photoreactors design and concepts vary based on the working regime (static or dynamic), photocatalyst morphology (powders or bulk) and liquid volume [60–62]. The photoreactors using suspension photocatalysts benefit from the advantage of the simple design and high specific photocatalyst surface area. The disadvantage is represented by the difficulties on catalyst recovery and reuse and the shadow effect of the catalyst, which

may reduce the light penetration during the photocatalytic activity. The photoreactors working with immobilized photocatalysts (fibers [63], fixed bed reactors [64], packing bed and monolith [65]) have the advantage of easy operation procedures and catalyst recovery. However, the uniform distribution of the photocatalyst in the wastewater volume is still a challenge to be addressed. The mass transfer and reaction kinetic data resulting from experiments can be used together with computational fluid dynamic methods to optimize important photoreactors set-up parameters: the reactor room geometry or operation parameters (flow rate, irradiation period, etc.) [66–68].

Therefore, the experimental and numerical methods can be coupled to provide input data for the photoreactors development, adapted for a particular type of pollutants and volume, in order to be sustainable and cost effective.

3. Photoreactors Design and Concepts

The photoreactors can be characterized based on several parameters: geometrical shape, photocatalyst type or morphology, fluid dynamics or applications. The present paper focus on two most common photoreactor geometrical shapes: cylindrical and rectangular. The analysis includes the influence of flow rate, reactor volume, light properties, photocatalyst and pollutant characteristics (dosage, concentration, etc.) on the overall photocatalytic efficiency of the process. Due to the length limitation, the mini-review cannot include all the representative papers published until now. The papers containing insufficient relevant data or missing experiments were excluded.

3.1. Cylindrical Photoreactors

The cylindrical reactors are usually irradiated by a central lamp or lamps arranged in a circle (Figure 3). The photocatalyst can be dispersed into the liquid volume or immobilized on various substrates (including the lamp cover). Additionally, the set-up often contains a storage tank (with aeration and mixer), pumps, valves, flowmeter and a control system able to manage the entire system. The storage tank aeration is required to ensure oxygen saturation conditions during the oxidative radical's formation. The cylindrical reactors have the advantage of radial flow distribution, which increases the diffusion homogeneity of the mobile photocatalysts. Table 1 present representative studies regarding the employment of cylindrical reactors in the photocatalytic removal of different organic pollutants (phenols, pharmaceutical active compounds, dyes, etc.).

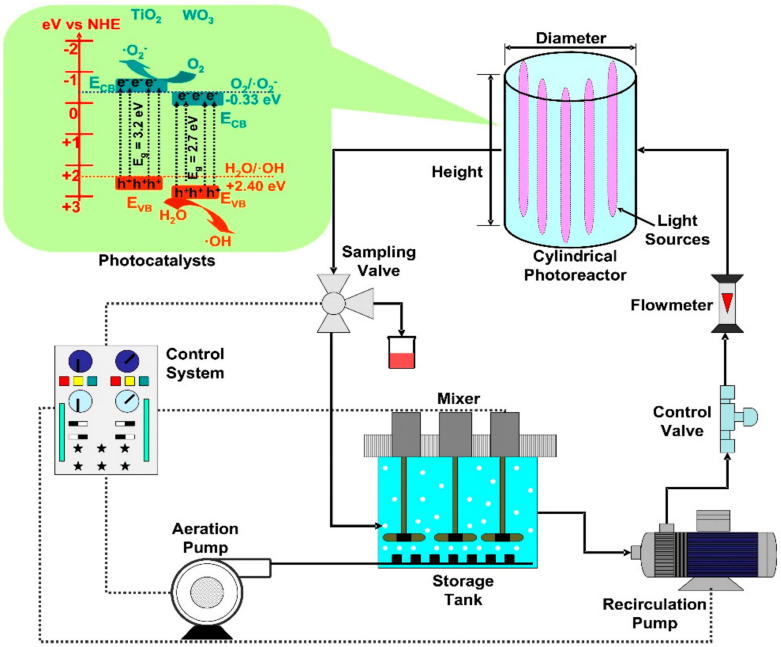

Figure 3. Cylindrical photoreactors components (TiO_2/WO_3 heterostructure photocatalyst).

Table 1. Cylindrical photoreactors parameters for wastewater treatment.

Photoreactor		Radiation Parameters				Photocatalyst Material and Dosage	Photocatalysis			Ref.
Working Regime	Volume (L)	Flow Rate L/min	Spectra	Intensity (W)	Period (min)		Pollutant	Concentration (mg/L)	Efficiency (%)	Constant Rate (h^{-1})	
Dynamic/Flow	4.9	19	UV-A	60	240	TiO_2 350	Phenol	20	15.8	0.041	[69]
						TiO_2 3000			55.7	0.205	
				90		TiO_2 350			21.7	0.06	
						TiO2 3000			49	0.171	
Dynamic/Flow	3.3	2	UV	40	150	TiO_2 100	Phenol	30	100	np *	[70]
Dynamic/Flow	1.06	6.0	UV-C	11	300	TiO_2 Np	p-Nitrophenol	15	95.7	0.611	[71]
Dynamic/Stirring	0.15	nr **	UV	90	15	TiO_2 0.55	4-nitrophenol	10	80	np	[72]
Dynamic/Flow	0.34	0.05	UV-Vis	1000	300	g-C_3N_4/chitosan 0.1	Sulfamethoxazole	25	30	0.096	[73]
							Carbamazepine	23	10	0.042	
							Phenol	9.4	20	0.06	
Dynamic/Flow	1.6×10^{-2}	0.83	UV-C	11	120	Direct photolysis aid with H_2O_2 100 Mm	Oxytetracycline	20	97	np	[74]
Dynamic/Stirring	3	nr	UV	16	15	Direct photolysis aid with H_2O_2 10 mM	Sulfamethazine	10	100	0.315	[75]
Dynamic/Flow	1×10^{-4}	0.01	UV	8	2	Direct photolysis	Benzoylecgonine	9.1	100	np	[76]
Dynamic/Stirring	0.12	nr	UV-C	9	60	Direct photolysis aid with $S_2O_8^{2-}$ 0.36	Acetaminophen	50	84.3	0.027	[77]
Dynamic/Flow	0.44	0.07	UV	5.7	60	Fe(II) 0.05 and peroxymonosulfate 20	Metformin	50	99	0.014	[78]
Dynamic/Flow	0.2	144 ncc/min	UV	14	240	ZnO 0.41	Caffeine	12.5	100	0.0196	[79]
							Paracetamol	12.5	77	np	

Table 1. *Cont.*

Photoreactor		Radiation Parameters			Photocatalyst Material and Dosage	Photocatalysis			Ref.
Working Regime	Volume (L)	Flow Rate L/min	Spectra	Intensity (W)	Period (min)		Pollutant	Concentration (mg/L)	Efficiency (%)	Constant Rate (h^{-1})	
Dynamic/Flow	14.4	24	Sunlight	15.17	70	TiO_2 0.25	Methylene blue (MB)	10	99	np	[80]
						TiO_2 0.5	4-chlorophenol		55		
Dynamic/Flow	7.7	12	UV	np	120	TiO_2 0.5	Methyl red	10	99.5	0.05	[81]
Dynamic/Stirring	0.5	nr	UV	125	140	TiO_2 100	Direct Red	30	100	0.07	[82]
					240			40	100	0.04	
Dynamic/Stirring	3	nc	UV	16	60	$Na_2S_2O_8$ 1.92	Reactive Red	100	100	np	[83]
Dynamic/Flow	np	2.7	Vis	150	60	N-doped $TiO_2$0.7	Methyl orange (MO)	5	59.3	0.03	[84]
Dynamic/Flow	0.8	0.05	UV	10	720	TiO_2 Np	Rhodamine B	10	91	0.032	[85]
							MO	10	69	0.026	
Dynamic/Flow	1.41	16.1	UV	100	60	TiO_2 400	Oxalic acid	0.9	80	np	[86]
Dynamic/Flow	np	2.5	UV-C	16	180	TiO_2:SiO_2 np	Paraffin	500	86	2.5	[87]
Dynamic/Flow	6	0.5	UV	13	150	Direct photolysis aid with H_2O_2 0.9	Poly(vinyl alcohol)	20	63	np	[88]

* not provided; ** not required.

The phenol removal was evaluated using 4.9 L [69] and 3.3 L [70] reactors and TiO_2 as the photocatalyst. The 4.9 L reactor use a flow rate of 19 L/min and the irradiation was done by a UV-A light source able to provide 60 or 90 W intensity. The highest efficiency (55.7%) was recorded when the TiO_2 dosage was 3000 mg and the light irradiation was 60W. Using the same photocatalyst dosage, phenol concentration (20 mg/L) and irradiation period (240 min) but higher light intensity (90 W) the photocatalytic efficiency exhibit 49% showing that there is no linear dependence between the photocatalytic pollutant removal and the UV-A light intensity. Basically, at low values of light intensities, the rate of photogenerated electron-hole formation increases and the rate-limiting step is represented by the holes formation. Higher light intensities may induce loss of photonic efficiency due to excessive heating of the reaction solution. However, higher concentration of phenol (30 mg/L) was completely removed by using a 3.3 L reactor with a flow rate of 2 L/min. The results confirm that lower UV light intensity (40 W) and TiO_2 dosage can improve the photocatalytic efficiency due to better light penetration into the aqueous environment. The photocatalyst immobilized on rotating substrate will increase the mass transfer favoring the phenol degradation. Similar experiments were done on 4-nitrophenol but in very different experimental conditions. Low UV-C light intensity (11 W) was used to irradiate a 1 L reactor [71] during 300 min. At a flow rate of 6 L/min the photocatalytic efficiency toward 4-nitrophenol (15 mg/L) removal in the presence of TiO_2 was 95.7%. When the flow rate increases, the liquid phase turbulence increases too, which provide a considerable reduction of the mass transfer resistance in the liquid, simultaneously with the appetency of renewing the photocatalyst surface due to the contaminants diffusion. Using a 0.15 L small reactor size [72], lower 4-nitrophenol concentration (10 mg/L) and higher light intensity (90 W) the photocatalytic efficiency after 15 min of irradiation was 80%. These results can be used for large applications considering the energy sustainability as a prerequisite on developing new cost-effective technologies.

A comparative study between the phenol and pharmaceutical active compounds photocatalytic removal was done using a 0.34 L reactor, 0.05 L/min flow rate and g-C_3N_4/chitosan mediators [73]. After 300 min of irradiation with 1000 W UV–Vis light source, the photocatalytic phenol removal was 20%, while for carbamazepine was 10% and for sulfamethoxazole was 30%. However, it is worth mentioning that the pharmaceutics compounds concentration was double compared with phenol concentration. The influence of a slow mass transfer rate on carbamazepine and sulfamethoxazole photodegradation was more predominant, while the g-C_3N_4 coverage by chitosan has a detrimental impact on phenol degradation. The influence of direct photolysis of oxytetracycline [74] and sulfamethazine [75] pharmaceutics compounds was evaluated under UV irradiation. The microreactor with a volume of 1.6×10^{-2} L exhibit 97% oxytetracycline photocatalytic removal after 120 min of irradiation with 11 W UV-C light. The photocatalytic system uses 20 mg/L oxytetracycline concentration and 100 mM of H_2O_2. The increase in flow rate from 50 to 100 Lh^{-1} will reduce the antibiotic residence time inside the photoreactor. To overcome this aspect the recirculation's number can be increased considering the overall energetic balance of the photocatalytic system. Using a larger reactor of 3 L, the 10 mg/L sulfamethazine solution was completely removed after 15 min of irradiation with 16 W UV light source. The study indicate that the photocatalytic efficiency improves when the H_2O_2 concentration increased from 1 to 10 mM due to more ·OH radicals available to participate in the sulfamethazine mineralization. If the H_2O_2 concentration increases up to 20 mM then the photocatalytic efficiency decreases as H_2O_2 excess acts as a scavenger for ·OH, generating ·OOH groups.

A microreactor with 1×10^{-4} L volume was tested for the direct photolysis of benzoylecgonine [76], a cocaine metabolic product formed by the liver and excreted in the urine. The experimental tests were done at 0.01 L/min flow rates using a low intensity (8 W) UV light source. After 2 min of irradiation the 9.1 mg/L benzoylecgonine concentration was completely removed from the aqueous solution. These results indicate that cylindrical microreactor can be efficiently used for the removal of the metabolic product without the

addition of oxidative species and having low energy consumption. The key parameter is the optimized flow rate in accordance with the pollutant concentration, reactor size and light intensity. Two pharmaceutical compounds, acetaminophen [77] and metformin [78], with the same concentration (50 mg/L) were submitted to photodegradation during 60 min of irradiation. The acetaminophen solution was tested in a 0.12 L reactor under continuous stirring and using a 9 W UV-C radiation source. The metformin degradation was evaluated into a 0.44 L reactor using 0.07 L/min flow rate and 5.7 W UV radiation source. The direct photolysis of acetaminophen aid by $S_2O_8^{2-}$ (0.36 mg/L) reached 84.3% removal efficiency due to the $SO_4^{-}\cdot$ production through a proton-catalyzing process. In the case of metformin photodegradation the photocatalytic process was mediated by Fe(II) (0.05 mg/L) and peroxymonosulfate (20 mg/L). The flow rate was adapted according with the rector volume (0.44 L) at 0.07 L/min. Around 99% of the metformin was removed after 60 min of irradiation with a 5.7 W UV light source confirming the enhancement of the degradation performance due to the increased concentration of oxidative radicals. The addition of Fe(II) into the reaction medium will induce parallel Fenton reaction, producing additional HO· and $HO_2\cdot$ radicals with positive impact on metformin degradation. Figure 4 indicate the contribution of all participants into pollutant removal during the photocatalytic activity. The photoreactor set-up was optimized to provide certain quantity of mediator and to allow even distribution and perpendicular incidence of UV light.

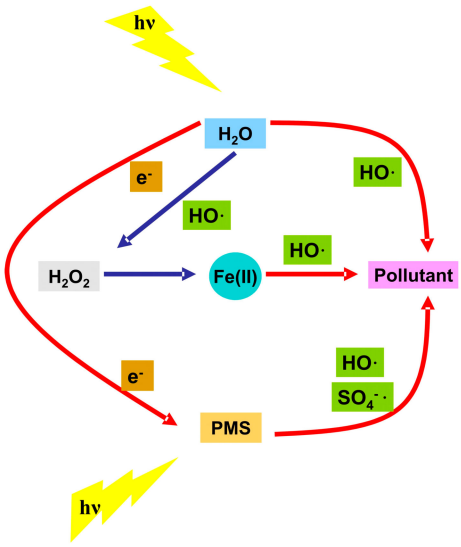

Figure 4. Generation of oxidative species during the pollutant removal.

Zinc oxide (ZnO) was employed as a photocatalyst for paracetamol and caffeine removal using a 0.2 L reactor [79]. Both reference pollutant solutions were kept at the same concentration (12.5 mg/L) and photocatalyst dosage. The samples were irradiated for 240 min with a 14 W UV light source and at a constant flow rate of 144 Ncc/min. The results indicate the complete removal of caffeine, while the paracetamol concentration was reduced with 77%. The cause of the photocatalytic activity differences toward caffeine and paracetamol were not completely elucidated. The influence of surface chemistry and pollutant molecule stability play an important role on the mineralization process. The investigation done on floating and fixed-bed indicate the advantages of flotation, able to ensure uniform ZnO irradiation, which produce more oxidative radicals required for pollutant degradation. A high reactor volume (14.4 L) was tested for a comparative investigation regarding 4-chlorophenol and methylene blue (MB) removal [80]. The pollutant concentration was similar (10 mg/L) but the TiO_2 photocatalyst dosage varied from 0.25 for MB to 0.5 mg/L for 4-chlorophenol. The same working conditions were applied: 24 L/min flow rate and 70 min of sunlight irradiation. The reactor set-up includes the storage tank, a centrifugal pump and two control valves required to set the recirculation flow rate. The higher

MB photodegradation efficiency (99%) comparing with 4-chlorophenol (55%), confirms the previous investigations [69,73] showing that the phenol compounds are more reluctant to the oxidative radicals' activity during the photocatalyst light irradiation. Additionally, the results indicate that the degradation increases at higher initial contaminants concentration since the reaction order is above zero. Considering the use of direct solar radiation, the set-up can be easily scaling up for large applications.

A flow reactor and stirring dynamic reactors were used to remove methyl red [81] and direct red [82] dyes in the presence of TiO_2 photocatalyst. The flow dynamic reactor has 7.7 L volume and uses TiO_2 catalyst to remove 10 mg/L methyl red pollutant. After 120 min of irradiation and using 12 L/min flow rate the photoreactor was able to degrade 99.5% of methyl red. Optimizing the catalyst dosage based on the photoreactor technical parameters can significantly decrease the chemicals consumption during the photocatalytic activity. The second reactor working in continuous stirring process has a lower volume (0.5 L) and use a high TiO_2 dosage. The experiments involve two direct red dye concentrations: 30 mg/L and 40 mg/L. The photocatalytic evaluation indicates an interesting dependence between the dye concentration and irradiation period required to completely eliminate the pollutant. The 30 mg/L pollutant concentration was removed in 140 min, while for the mineralization of 40 mg/L direct red the exposure time increases at 240 min. Consequently, the energy consumption must be correlated with the pollutant concentration in order to ensure the implementation of a cost-effective technology. At high dyes concentrations, the solution become more colored acting as light screening for the irradiation sources. A 3.0 L reactor was also used to evaluate the reactive red dye degradation under continuous stirring [83]. The degradation of 100 mg/L reactive red solution was mediated by $Na_2S_2O_8$ under 16 W UV radiation source. After 60 min of irradiation the reactive red was completely eliminated. This type of photoreactor has the advantage of working at high pollutant concentration due to the oxidative activity of $SO_4^{-}\cdot$ radicals formed during UV irradiation with 254 nm wavelength. These results indicate the importance of adapting the light source characteristic at a specific pollutant and mediator's compounds and a particular dynamic regime. The stirring reactor has the advantage of keeping the solution and light radiation in permanent contact, without requiring the solution recirculation through pipes and storage tank.

The methyl orange (MO) photocatalytic removal was performed under irradiation with 150 W Vis light [84] and 10 W UV light [85] sources. In the Vis irradiation scenario, the MO concentration was 5 mg/L and the TiO_2 photocatalyst was doped with N to extend the light absorbance spectra. After 60 min of irradiation and using a 2.7 L/min flow rate, the photocatalytic efficiency of MO removal reaches 59%. By switching to UV irradiation scenario and undoped TiO_2, the photocatalytic efficiency at a lower flow rate (0.05 L/min) and longer exposure time (720 min) increases at 69%, even if the MO concentration was double (10 mg/L). The results were verified on Rhodamine B and the photocatalytic activity increased at 91% in the same experimental conditions. The comparative evaluation indicates that the energy consumption in the UV scenario (120 Wh) was lower than that of Vis light scenario (150 Wh), which use a smaller MO concentration. The energy consumption for the MO degradation using a slurry flow photoreactor is drastically reduced by optimizing the catalyst dose in correspondence with the light scenario and the provided turbulence.

Cylindrical reactors were employed for the removal of oxalic acid [86], paraffin [87] and poly(vinyl alcohol) [88] under UV irradiation. The oxalic acid solution with 0.9 mg/L concentration was inserted into a 1.4 L reactor together with 400 mg/L TiO_2 dosage. Keeping a constant flow rate of 16 L/min during 60 min of irradiation with 100 W UV source it was possible to remove 80% from the initial oxalic acid concentration. While lamp orientation showed minimal photocatalytic impact, the reactor volume and flow rate may induce significant changes on the overall pollutant removal efficiency. Larger reactor and high flow rates seem to boost the photocatalytic activity due to a lower density of catalyst particles and higher irradiated surface. TiO_2/SiO_2 heterostructure was used as photocatalysts for the removal of high concentrated paraffin (500 mg/L) solution. The

irradiation was done with a 16 W UV-C light source and the flow rate was lower (2.5 L/min) compared with oxalic acid experiments. After 180 min of irradiation, the photocatalytic efficiency was 86%, which shows that changing one of the key parameters (photocatalyst composition, pollutant type or concentration and irradiation source) it is possible to modify the degradation reaction kinetics based on the system capability to produce oxidizing radicals. The poly(vinyl alcohol) solution with 20 mg/L concentration was placed into a 6 L (0.5 L/min flow rate) reactor and submitted to direct photolysis aided by 0.9 mg/L H_2O_2. The photocatalytic efficiency reaches 63% after 150 min of irradiation with 13 W UV light source. Direct photolysis can represent a good alternative to photocatalysis, considering the catalysts limitations in terms of active surface and interface chemistry. However, the excessive use of photolysis promoters (i.e., H_2O_2 and $S_2O_8^{2-}$) raises serious issues in terms of a green approach and environmental impact.

The cylindrical photoreactors can be fully integrated into large scale wastewater treatment technologies by optimizing the geometrical configuration with the irradiation scenario, pollutant characteristics and technical parameters. Higher reactor volumes and flow rates must consider the energy consumption as a key parameter for proposing a cost-effective technology. A significant limitation is represented by the inability to predict the variation of photocatalytic activity based on the pollutant type and interface chemistry with the catalysts.

3.2. Rectangular Photoreactors

The rectangular reactors allow a higher versatility of the irradiation sources orientation, which can be placed on the internal lateral sides (Figure 5), central position, horizontal or vertical in the corners. The immobilized photocatalysts can be placed on the reactor walls, on the lamps cover or even on individual substrates (e.g., glass, textiles, and composites). If mobile photocatalysts are employed, the flow rate must be adapted to this particular geometry in order to provide a homogenous diffusion through the reactor volume. Consequently, the photoreactor set-up components are chosen to ensure a maximum production of oxidative species required to remove the organic pollutants. Table 2 includes representative studies on the photocatalytic applications of rectangular reactors for the removal of various organic pollutants.

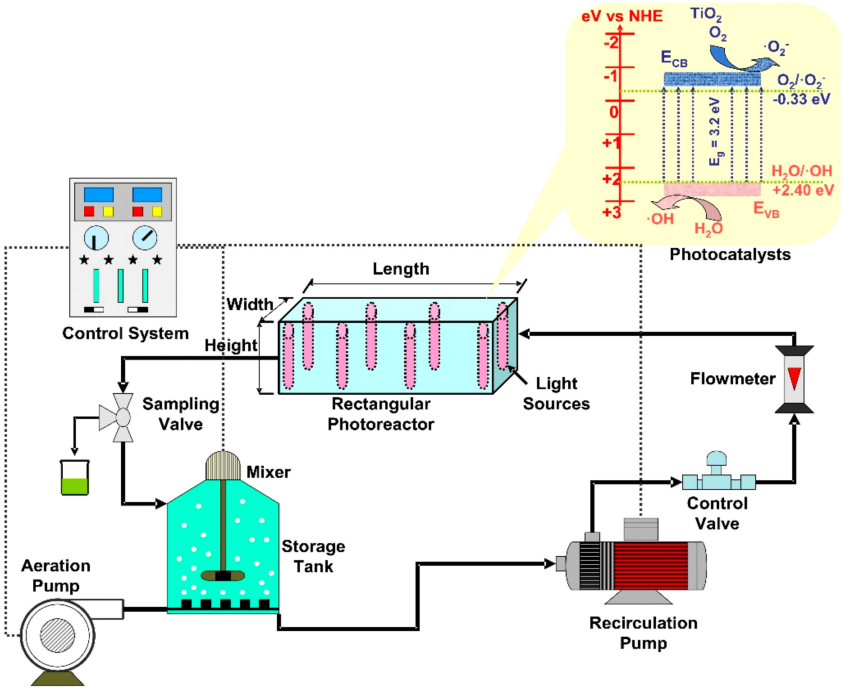

Figure 5. Rectangular photoreactors components (TiO_2 photocatalyst).

Table 2. Rectangular photoreactors parameters for wastewater treatment.

Photoreactor		Radiation Parameters				Photocatalyst Material and Dosage	Photocatalysis				Ref.
Working Regime	Volume (L)	Flow Rate L/min	Spectra	Intensity (W)	Period (min)		Pollutant	Concentration (mg/L)	Efficiency (%)	Constant Rate (min^{-1})	
Dynamic/Flow	0.375	0.04	UV	8	264	N-doped TiO_2 372	MB	32	75	np*	[89]
Dynamic/Flow	0.3	0.15	Vis	36	180	N-doped TiO_2 Np	MB	7	70	np	[90]
Dynamic/Flow	3.4	7.25	Sunlight	np	2880	TiO_2 0.9	MB	25	98	np	[91]
Dynamic/Flow	1.25	3.44	Sunlight	np	2880	TiO_2 0.5	MB	25	96	8×10^{-4}	[92]
	3.25				2880	TiO_2 0.9			97	0.002	
Dynamic/Oscillatory	0.1	nr **	UV	4	110	ZnO 100	MB	10	100	0.05	[93]
Dynamic/Stirring	0.003	nr	UV	5	30 500	ZnO, H_2O_2 200	MB salicylic acid	0.013 0.013	100 100	0.097 0.0057	[94]
Dynamic/Flow	0.066	0.033 0.033 0.067	UVA Vis	8	240	Ag-modified TiO_2 1	Salicylic acid	27.6	90 92 100	np	[95]
Dynamic/Stirring	0.5	nr	Vis	15	240	C-N-S tridoped TiO_2 1	Penicillin G	5	95	0.016	[96]
Dynamic/Flow and Stirring	0.6	0.09	UV	30	np	TiO_2 0.36/face	Flumequine	20	93	0.2	[97]
Dynamic/Flow	0.5	0.03	Sunlight	np	100	ZnO Np	Reactive red	118	100	np	[98]
Dynamic/Flow	1.0	1.68	UV	np	300	TiO_2 Np	Tartrazine	10 20 30	77.77 57.72 46.57	0.3 0.18 0.15	[99]
Dynamic/Flow and Stirring	0.15	0.032	Vis	np	480	N and S-doped TiO_2 Np	Basic Yellow Basic Red Basic Blue	25	65 78 98	np	[100]
					240	Zn, N and S tri-doped TiO_2 Np	Basic Yellow Basic Red Basic Blue	25	88 94 99		
Dynamic/Flow	0.075	0.04	Vis	60	200	N-doped TiO_2 0.6	E. coli	106 colony-forming units mL^{-1}	50	0.067	[101]
Dynamic/Flow	4.5	6	Vis	40	3600	W-C-codoped TiO_2 8.47	Leachate	550	84	0.0191	[102]
Dynamic/Stirring	1.5	nr	UV-A	120	350	TiO_2 0.2	Hexacyanocobaltate	32	40	0.0021	[103]

Table 2. *Cont.*

Photoreactor		Radiation Parameters				Photocatalyst Material and Dosage	Photocatalysis				Ref.
Working Regime	**Volume (L)**	**Flow Rate L/min**	**Spectra**	**Intensity (W)**	**Period (min)**		**Pollutant**	**Concentration (mg/L)**	**Efficiency (%)**	**Constant Rate (min^{-1})**	
Dynamic/Flow	0.04	np	UV-A	15	90	TiO_2 1	Potassium hexacyanoferrate	100	70	np	[104]
Dynamic/Flow	5	0.55	UV	14.4	60	UiO-66(Ti)-Fe_3O_4-WO_3 0.125	Ammonia	30	91.8	0.903	[105]
Dynamic/Flow	6	7.8	UV	5	360	TiO_2 0.5	p-nitrophenol	50	71.91	0.118	[106]
Dynamic/Flow	0.3	np	Sunlight	np	300	TiO_2 Np	Bisphenol A	0.45	78.7	0.036	[107]
							17 β-estradiol	0.54	83.7	0.051	
							17 α-ethynyl estradiol	0.59	79.7	0.059	

* not provided; ** not required.

N-doped TiO_2 photocatalyst immobilized on glass spheres was involved in the photocatalytic MB removal using two rectangular reactors with different volumes. The 0.375 L reactor [89] with 0.04 L/min flow rate was irradiated for 264 min with an 8 W UV light source. The photocatalytic set-up was able to remove 75% from the 32 mg/L MB initial concentration. Due to the flat profile, a plug flow behavior providing a perfect homogenization of the inside fluid was obtained. The presence of structured catalyst will increase the removal rate due to the higher surface exposure to light irradiation. The second reactor has a volume of 0.3 L [90] and work in a higher flow rate (0.15 L/min). The photocatalytic efficiency after 180 min of irradiation with a 36 W Vis light source was 70%. However, in this case the MB, the concentration was 4.5 × lower, and the energy consumption was 3× higher. These values indicate the necessity of adopting the most suitable irradiation scenario and flow rate, able to favor the oxygen readsorption on the photocatalyst surface, which could subsequently react with the excess of photogenerated electrons, hence reducing recombination with holes.

Direct exposure to sunlight can be an energy efficient method for MB removal using TiO_2 as a photocatalyst. A 3.4 L reactor [91] was used to evaluate the photocatalytic efficiency toward 25 mg/L MB solution and the flow rate was established at 7.25 L/min. Around 98% of the MB was removed after 48 h of sunlight exposure, considering that the photoreactor efficiency depends on the ratio between the reactor volume to the total solution volume. A larger ratio of volume will be beneficial, allowing the increase of the catalyst surface (when is immobilized) and leading to a higher photodegradation ability of the photoreactor. These results were confirmed when the same MB concentration was tested in 3.25 and 1.25 L reactors [92] using a flow rate of 3.44 L/min. The photocatalytic efficiency after 48 h of sunlight exposure shows a small decrease at 97% for 3.25 L reactor and 96% for 1.25 L reactor. These photocatalytic efficiency differences become quantitatively significant when the technology is scaled-up for a large application. Comparing the rate constants of both photoreactors shows that the 3.25 L reactor (0.117 h^{-1}) was twice faster in removing the MB pollutant, than the 1.25 L reactor (0.05 h^{-1}). The use of sunlight represents an alternative for implementing sustainable technologies but is dependent on the geographical position and climatic changes.

An oscillatory [93] and a dynamic [94] reactor was employed for MB removal using ZnO photocatalyst. The oscillatory reactor has a volume of 0.1 L and works using a low intensity (4 W) UV light source. The 10 mg/L MB solution was completely removed in the presence ZnO after 110 min of irradiation. The oscillatory motion will minimize the catalyst particles deposition and increase the suspension leading to an improvement of the photocatalytic activity. An additional argument is given by the lower hydraulic resistance of the oscillatory motion, combined with a longer resilience period of the liquid in reactor room. The dynamic microreactor with 3×10^{-3} L volume use a higher ZnO dosage, and the photocatalytic activity is aid by H_2O_2. Low MB concentration (0.013 mg/L) was completely removed after 30 min of irradiation with a 5 W UV source. The same result was obtained for salicylic acid (0.013 mg/L) removal but after 500 min of irradiation. The results shows that the removal reaction rate for MB is 17 × higher compared with salicylic acid, confirming the photocatalytic efficiency depends on the pollutant molecule characteristics. Using a microreactor bring the advantage of: (1) low quantities of reactants, solvents and catalyst; (2) safe conditions for UV radiation utilization; (3) energy saving and (4) facile operation of the set-up. The photocatalytic removal of high salicylic acid concentration (27.6 mg/L) was tested in a 6×10^{-2} L dynamic reactor using different flow rates and irradiation sources [95]. The highest photocatalytic activity (100%) in the presence of 1 mg/L Ag modified TiO_2 was obtained after 240 min of irradiation with the 8 W Vis source and using a flow rate of 0.067 L/min. The photocatalytic efficiency decreased at 92% by reducing the flow rate up to 0.033 L/min. By keeping the same flow rate (0.033 L/min) but changing the radiation sources from Vis to UV (same intensity) the photocatalytic efficiency decreased by 90%. Besides doping, silver can be used to form Schottky junctions (Figure 6) able to generate high concentration of oxidative species, enhancing the photocatalytic reactions.

In a reaction system mediated by mobile photocatalytic particles, the volumetric photon absorption is a key parameter to increase the local reaction rates. Assuming a uniform distribution of TiO_2 particles in the liquid environment, the matches between catalyst particles local velocity and the fluid local velocity in laminar flow will ensure a longitudinal direction of the photocatalyst particles. Hence, to avoid poor illumination regions it is important to properly design the width of rectangular reactors.

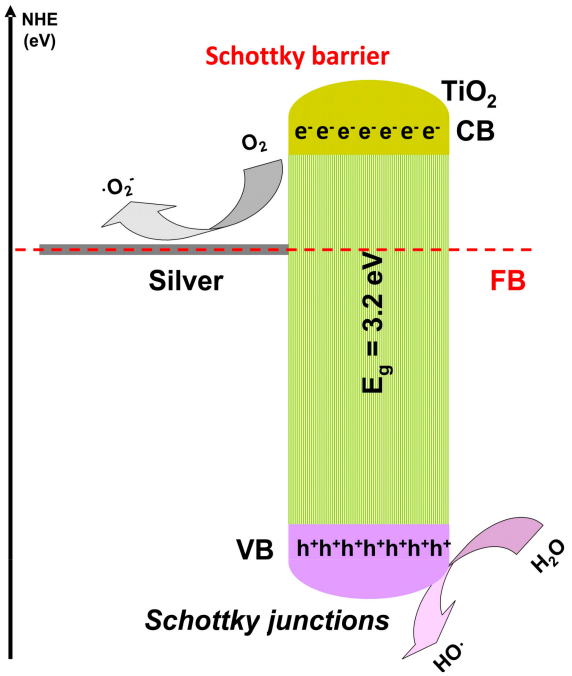

Figure 6. Oxidative species generation using Schottky junction.

The photodegradation of two antibiotics (penicillin G and flumequine) were tested in the presence of the TiO_2 photocatalyst. Penicillin G solution with 5 mg/L concentration was inserted into a 0.5 L reactor, working under continuous stirring [96]. The TiO_2 photocatalyst was simultaneously doped with C, N and S in order to increase the absorption range in Vis spectra. After 240 min of irradiation with 15 W Vis light spectra, 95% of penicillin G was removed. The penicillin G degradation efficiency increased based on the permeate water volumetric percent recycled by the photoreactor, due to the prolonged hydraulic residence time. The flumequine solution was tested at a 4× higher concentration (20 mg/L) in a 0.6 L reactor using a double flow rate (0.09 L/min) and stirring regime [97]. The TiO_2 photocatalyst was immobilized on 30 × 10 cm^2 textile substrates, with 0.36 g of TiO_2 per textile face. Around 93% of flumequine was removed using a 30 W UV radiation source. These results indicate that low transmittance substrates can be successfully involved in the photoreactor set-up development, with the condition of ensuring a homogeneous irradiation on the entire substrate surface. Using luminous textile has the advantage of removing the catalyst separation process from the treated solution, and allows the photoreactor size reduction by light source integration in the photocatalytic support.

High concentrated reactive red solution (118 mg/L) was submitted to photodegradation in a 0.5 L reactor under sunlight irradiation [98]. The ZnO photocatalyst was used in form of a thin film coated on a glass substrate. The experiments made 0.03 L/min flow rate indicate that the time required to remove half of the reactive red concentration was 15.8 min and the complete removal was achieved in 100 min. Tartrazine dye solution with different concentrations (10, 20 and 30 mg/L) was tested in a 1 L reactor volume using the TiO_2 catalyst and UV radiation [99]. After 300 min of irradiation the experiments indicate the dependence between pollutant concentration and photocatalytic efficiency: the reaction rate was double at 10 mg/L concentration than that of 30 mg/L, and 1.66× higher than that

of 20 mg/L. Consequently, 77.7% of reactive red was removed at the lowest concentration and only 46.5% at the highest concentration. The degradation rate was correlated with the catalyst active surface, responsible for electron-hole pair's photogeneration. In this particular case, the amount of catalyst was constant, and the hydroxyl radical's concentration remains unchanged, while tatrazine dye concentration increases. Therefore, the available hydroxyl radical for each tartrazine molecules decreased with increasing the dye concentrations, leading to lower photodegradation efficiencies. Higher tartrazine concentrations will increase the liquid UV light screening, which is an additional contributor on the decreasing of the hydroxyl radical's amount. When the flow rate increase from 9.78 to 28 mL/s, the degradation efficiency increases, due to a higher turbulence in the solution, promoting the external mass transfer from the dye solution to photocatalyst surface. A complex study was made to verify the influence of dye molecule, photocatalyst and irradiation exposure period on the photocatalytic activity of a combined flow (0.032 L/min) and stirring reactor with 0.15 L volume [100]. In the first step, basic yellow, red and blue dyes with 25 mg/L concentration were irradiated for 480 min with Vis light in the presence of N and S-doped TiO_2. In the second step the same dyes concentrations were irradiated for 240 min with Vis light but using Zn, N and S tri-doped TiO_2 catalyst. The results indicate similar photocatalytic efficiency for basic blue dye in both cases. However, for basic red and yellow there was a significant increase of the photocatalytic activity in the second scenario (from 68 to 88% for basic red and from 78 to 94% for basic yellow). These variations of the photocatalytic response can be the result of anions doping, such as nitrogen and sulfur in the TiO_2 anatase structure, inducing changes of the electrical conductivity or optical properties due to anions p orbitals combination with oxygen 2p orbitals, hence lowering the bandgap energy. Adding Zn as codoping will play the role of electron scavenger, with beneficial consequences on preventing the electron-hole recombinations. The insertion of Zn^{2+} ions in TiO_2 anatase lattice enhance the $HO\cdot$ and $O_2{}^{-}\cdot$ production, playing a significant contribution in the dye degradation.

The photocatalytic removal of 10^6 colony-forming units/mL was evaluated in a rectangular 0.075 L reactor using a flow rate of 0.04 L/min [101]. The sample was irradiated with Vis light (60 W) for 200 min in the presence of N-doped TiO_2 photocatalyst. The 50% photocatalytic efficiency was obtained after the optimization of *E. coli* concentration and flow rate. The study shows that by reducing the *E. coli* concentration at half of the above value, the photocatalytic activity decreased due to the minimum close proximity between the bacteria and immobilized N-doped TiO_2 nanoparticles surface. The flow rate influence was statistically significant, indicating that by increasing the flow rate up to 0.06 L/min the photocatalytic efficiency decreased with more than 20%. This variation is related with the decrease in residence time of the *E. coli* solution due to the increase in flow rate, inducing an insufficient contact between the bacteria colony and immobilized photocatalyst. Landfill leachate (550 mg/L) considered as recalcitrant wastewater was photocatalytically treated in a 4.5 L reactor using W-C-codoped TiO_2 layers as a catalyst [102]. The W-C-codoping allow the TiO_2 catalyst to be active in the Vis range, which is considered as an advantage when passing to sunlight is envisaged. After 60 h of irradiation with 40 W Vis light source and using a flow rate of 6 L/min the photocatalytic efficiency reached 84%. The photocatalyst morphology in the reactor plays an important role on the overall photocatalytic activity. In the presence of catalyst nanoparticles, two concurrencies' processes occur: adsorption and photodegradation. If the photocatalyst layer thickness increase, then it will reduce the adsorption mechanism for the nanoparticles located in the bottom layers. However, when the catalyst layer thickness is significantly higher than the optimum value, the porosity bottom layers will decrease, the nanoparticles become more compacted and the internal mass transfer is reduced.

UV-A radiation was used to remove hexacyanocobaltate [103] and potassium hexacyanoferrate [104] pollutants. A stirring reactor with 1.5 L volume was employed for the removal of 32 mg/L hexacyanocobaltate in the presence of 0.2 g of TiO_2. The reactor was irradiated with a high intensity (120 W) UV-A light source during 350 min in order

to decompose 40% of the initial hexacyanocobaltate concentration. Results show that the higher photocatalytic activity was obtained when extra oxygen was added into the reactor, since it generated higher free cyanide concentration and induced the oxidation chain up to NO_3^-, considering that reactive oxygen species are produced in the O_2 atmosphere. The potassium hexacyanoferrate removal (100 mg/L) was evaluated into a microreactor (0.04 L) using a low UV-A radiation intensity source (15 W) for a total period of 90 min. Due to the spatial limitation the TiO_2 dosage was reduced at 0.1 g and the photocatalytic efficiency was 70%. Using a higher potassium hexacyanoferrate concentration will induce a decrease of photocatalytic activity due to Fe precipitation on the TiO_2. These results are in accordance with other papers [94,95] employing microreactors, which exhibit high photocatalytic activity and possess better process control. However, these technologies raise issues when upscaling for large applications, due to unpredictable changes in term of parameters evolution (flow regime, uniformity, photo distribution, etc.).

Ammonia removal was tested in a large 5 L reactor volume, using UiO-66(Ti)-Fe_3O_4-WO_3 as a photocatalyst [105]. The flow rate was optimized at 0.55 L/min and after 60 min of irradiation with 14.4 W UV light source, 91.8% of the ammonia initial concentration (30 mg/L) was removed. At lower flow rates values, the catalyst diffusion in the reactor volume was insufficient while the catalyst residence time in the reactor room would increase, consequently more catalyst light exposure occurred. By increasing the flow rates above the optimized value, the convective mass transfer coefficient between the ammonia solution and photocatalyst surface was substantially enhanced, while the radiation contact time with the photocatalyst was reduced, which decreased the ammonia degradation efficiency. These experiments also highlighted that lower ammonia removal efficiency was obtained at higher pollutant concentration, due to the reduction of available catalyst active sites corresponding to each ammonia molecule.

Finally, rectangular photoreactors were tested for the removal of phenol compounds such as p-nitrophenol [106] and bisphenol A [107] in the presence of TiO_2 photocatalyst. The 50 mg/L p-nitrophenol solution was placed into a 6 L reactor, operating with a flow rate of 7.8 L/min. The sample was irradiated for 360 min with 5 W UV source light and the photocatalytic efficiency was 72%. Comparing with the experiments made in cylindrical reactors [71,72] the photocatalytic activity was significantly lower. However, it must be considered that in this case the light source intensity was lower and the pollutant concentration was higher. By increasing the TiO_2 catalyst amount, the available active sites will increase and the p-nitrophenol degradation is enhanced. On the other hand, high TiO_2 quantity will increase the solution opacity and light scattering effect reduces the formation of oxidative species. Additionally, TiO_2 particles tend to form an aggregate, which causes a reduction in the interfacial area between the catalyst and reaction solution. All these factors have a direct impact on the photocatalytic efficiency of the reactor set-up. The bisphenol A removal was evaluated in a smaller reactor (0.3 L) under direct exposure to sunlight for 300 min. The photocatalytic efficiency was 78.7% using low bisphenol A concentration. The experiments were repeated with 17 β–estradiol and 17 α-ethynyl estradiol, and the results were in the same range (83.7% for 17 β–estradiol and 79.7% for 17 α-ethynyl estradiol). These results indicate that using direct exposure to sunlight radiation can be a feasible way to remove organic pollutants. The main issues to this type of set-up are represented by the necessity to have a cooling system (to avoid overheating) and the unpredictability in term of light intensity.

The rectangular reactors can be easily upscaled based on a modular design, which allows the increase of solution volume treated each cycle. Due to the shape simplicity and geometrical versatility, the rectangular reactors can be implemented for small indoor or large outdoor applications. The main issues are related with optimizing the flow rate and irradiation parameters to avoid excessive velocities and to allow a uniform photocatalyst irradiation.

4. Conclusions and Perspectives

Both cylindrical and rectangular reactors bring advantages and disadvantages depending on the operation mode, irradiation sources, photocatalysts and pollutants parameters (concentration, composition, etc.). The photocatalytic set-up must optimize the reactor characteristics with the additional components in order to ensure a proper balance between the treated solution volume and the pollutant quantity removed at the end cycle. A high phenol concentration (30 mg/L) can be completely removed in a cylindrical reactor using low intensity UV sources (40 W) and short irradiation periods (150 min). Pharmaceutical compounds such as sulfamethazine (10 mg/L) can be completely removed in a stirring cylindrical reactor after 15 min of UV irradiation. Similar results were obtained by employing rectangular microreactors able to completely remove salicylic acid and MB dye using a 5 W UV light source.

The inappropriate photoreactor design could result in a significant increase of the energy consumption, inappropriate flow rate, uneven photon distribution or catalyst deactivation with direct implications on the photocatalytic efficiency. Optimizing the photoreactor design and technological parameters represents a continuous work and until now there are no clear regulations on what is the most suitable model to be applied in all cases.

In perspective, the photocatalytic reactors can be optimized by addressing two main issues: technical parameters and chemical characteristics. The ability to work under a wide range of liquid flow rates (avoiding turbulences and shear stresses that might damage the surface of the catalysts), efficient illumination system integration (high uniformity of the photon distribution on the photocatalytic surface), model simplicity and possibility to be easily configured for particular operation parameters are key points in the development of large size applications.

Several photocatalyst modifications can have a significant impact on the overall photocatalytic efficiency. Measures, such as surface metals/non-metals doping, metal-semiconductor coupling, surface photosensitization, semiconductors heterojunction or defect engineering will enhance the photocatalytic activity towards an organic pollutant. Coupling photocatalysis with other techniques such as membrane filtration, adsorption or biodegradation can boost the pollutant removal performance and represents alternatives for future applications.

The economic costs are essential for the implementation of large scale photocatalytic applications. The reactor design and technology must include a life cycle assessment, which may give certain inputs on the process feasibility. Often, small laboratory experiment fails when passing to large application due to the excessive costs. Simple's technologies, energy sustainability and environmentally friendly materials are a prerequisite when designing a reactor set-up.

Author Contributions: Conceptualization, A.E.; methodology, A.E.; software, A.E.; investigation, A.E.; resources, A.E.; data curation, A.E.; writing—original draft preparation, A.E.; writing—review and editing, A.E.; visualization, A.E; supervision, A.E.; project administration, A.E.; funding acquisition, A.E. All authors have read and agreed to the published version of the manuscript.

Funding: This work was supported by a grant of the Romanian Ministry of Education and Research, CCCDI-UEFISCDI, project number PN-III-P2-2.1-PED-2019-2028, within PNCDI III.

Data Availability Statement: Data presented in this study are available by requesting from the corresponding author.

Conflicts of Interest: The authors declare no conflict of interest.

References

1. Whitehead, P.G.; Bussi, G.; Hughes, J.M.R.; Castro-Castellon, A.T.; Norling, M.D.; Jeffers, E.S.; Rampley, C.P.N.; Read, D.S.; Horton, A.A. Modelling Microplastics in the River Thames: Sources, Sinks and Policy Implications. *Water* **2021**, *13*, 861. [CrossRef]
2. Xiao, L.; Liu, J.; Ge, J. Dynamic game in agriculture and industry cross-sectoral water pollution governance in developing countries. *Agric. Water Manag.* **2021**, *243*, 106417. [CrossRef]

3. Zhang, L.; Cui, B.; Li, L. Denitrification mechanism and artificial neural networks modeling for low-pollution water purification using a denitrification biological filter process. *Sep. Purif. Technol.* **2021**, *257*, 117918. [CrossRef]
4. Mashuri, S.I.; Ibrahim, M.L.; Kasim, M.F.; Mastuli, M.S.; Rashid, U.; Abdullah, A.H.; Islam, A.; Asikin Mijan, N.; Tan, Y.H.; Mansir, N.; et al. Photocatalysis for Organic Wastewater Treatment: From the Basis to Current Challenges for Society. *Catalysts* **2020**, *10*, 1260. [CrossRef]
5. Cao, X.; Wang, K.; Feng, X. Removal of phenolic contaminants from water by pervaporation. *J. Membr. Sci.* **2021**, *623*, 119043. [CrossRef]
6. Liu, Y.; Wang, J.; Song, P. Effects of electrolyzed water treatment on pesticide removal and texture quality in fresh-cut cabbage, broccoli, and color pepper. *Food Chem.* **2021**, *353*, 129408. [CrossRef]
7. Camargo-Perea, A.L.; Serna-Galvis, E.A.; Torres-Palma, R.A. Understanding the effects of mineral water matrix on degradation of several pharmaceuticals by ultrasound: Influence of chemical structure and concentration of the pollutants. *Ultrason. Sonochem.* **2021**, *73*, 105500. [CrossRef] [PubMed]
8. Ibrahim, I.; Belessiotis, G.V.; Arfanis, M.K.; Athanasekou, C.; Philippopoulos, A.I.; Mitsopoulou, C.A.; Romanos, G.E.; Falaras, P. Surfactant Effects on the Synthesis of Redox Bifunctional V_2O_5 Photocatalysts. *Materials* **2020**, *13*, 4665. [CrossRef]
9. McBeath, S.T.; English, J.T.; Graham, N.J.D. Circumneutral electrosynthesis of ferrate oxidant: An emerging technology for small, remote and decentralised water treatment applications. *Curr. Opin. Electrochem.* **2021**, *27*, 100680. [CrossRef]
10. Angelakis, A.N.; Vuorinen, H.S.; Nikolaidis, C.; Juuti, P.S.; Katko, T.S.; Juuti, R.P.; Zhang, J.; Samonis, G. Water Quality and Life Expectancy: Parallel Courses in Time. *Water* **2021**, *13*, 752. [CrossRef]
11. Li, D.; Zhuge, Y.; Ma, X. Reuse of drinking water treatment sludge in mortar as substitutions of both fly ash and sand based on two treatment methods. *Constr. Build. Mater.* **2021**, *277*, 122330. [CrossRef]
12. You, J.; Wang, L.; Zhao, Y.; Bao, W. A review of amino-functionalized magnetic nanoparticles for water treatment: Features and prospects. *J. Clean. Prod.* **2021**, *281*, 124668. [CrossRef]
13. Letshwenyo, M.W.; Mokgosi, S. Investigation of water treatment sludge from drinking water treated with Zetafloc 553I coagulant for phosphorus removal from wastewater. *J. Environ. Manag.* **2021**, *282*, 111909. [CrossRef]
14. Dudita, M.; Bogatu, C.; Enesca, A.; Duta, A. The influence of the additives composition and concentration on the properties of SnOx thin films used in photocatalysis. *Mater. Lett.* **2011**, *65*, 2185–2189. [CrossRef]
15. Tong, K.; Yang, L.; Du, X.; Yang, Y. Review of modeling and simulation strategies for unstructured packing bed photoreactors with CFD method. Renew. *Sustain. Energy Rev.* **2020**, *131*, 109986. [CrossRef]
16. Couto, C.F.; Lange, L.C.; Amaral, M.C.S. Occurrence, fate and removal of pharmaceutically active compounds (PhACs) in water and wastewater treatment plants—A review. *J. Water Proc. Eng.* **2019**, *32*, 100927. [CrossRef]
17. Zhao, W.; Chen, I.W.; Huang, F. Toward large-scale water treatment using nanomaterials. *Nanotoday* **2019**, *27*, 11–27. [CrossRef]
18. Stefán, D.; Erdélyi, N.; Vargha, M. Formation of chlorination by-products in drinking water treatment plants using breakpoint chlorination. *Microchem. J.* **2019**, *149*, 104008. [CrossRef]
19. Fatima, S.; Ali, S.I.; Iqbal, M.Z.; Rizwan, S. Congo Red Dye Degradation by Graphene Nanoplatelets/Doped Bismuth Ferrite Nanoparticle Hybrid Catalysts under Dark and Light Conditions. *Catalysts* **2020**, *10*, 367. [CrossRef]
20. Zhao, W.; Yang, X.; Liu, C.; Qian, X.; Wen, Y.; Yang, Q.; Sun, T.; Chang, W.; Liu, X.; Chen, Z. Facile Construction of All-Solid-State *Z*-Scheme g-C_3N_4/TiO_2 Thin Film for the Efficient Visible-Light Degradation of Organic Pollutant. *Nanomaterials* **2020**, *10*, 600. [CrossRef]
21. Zhao, D.; Zhang, X.; Zeng, X. Facile synthesis of MoO_3 nanospheres and their application in water treatment. *Mater. Lett.* **2019**, *256*, 126648. [CrossRef]
22. Li, X.; Cai, M.; Zhang, G. Evaluation survey of microbial disinfection methods in UV-LED water treatment systems. *Sci. Total Environ.* **2019**, *659*, 1415–1427. [CrossRef]
23. Ji, S.; Yang, Y.; Li, X.; Liu, H.; Zhou, Z. Facile Production of a Fenton-Like Photocatalyst by Two-Step Calcination with a Broad pH Adaptability. *Nanomaterials* **2020**, *10*, 676. [CrossRef]
24. Testolin, R.C.; Mater, L.; Radetski, C.M. Comparison of the mineralization and biodegradation efficiency of the Fenton reaction and Ozone in the treatment of crude petroleum-contaminated water. *J. Environ. Chem. Eng.* **2020**, *8*, 104265. [CrossRef]
25. Enesca, A.; Duta, A. The influence of organic additives on the morphologic and crystalline properties of SnO_2 obtained by spray pyrolysis deposition. *Thin Solid Film* **2011**, *519*, 5780–5786. [CrossRef]
26. Xie, A.; Cui, J.; Dai, J. Photo-Fenton self-cleaning PVDF/NH_2-MIL-88B(Fe) membranes towards highly-efficient oil/water emulsion separation. *J. Membr. Sci.* **2020**, *595*, 117499. [CrossRef]
27. Mazarji, M.; Minkina, T.; Dudnikova, T. Impact of humic acid on degradation of benzo(a)pyrene polluted Haplic Chernozem triggered by modified Fenton-like process. *Environ. Res.* **2020**, *190*, 109948. [CrossRef]
28. Fiorenza, R.; Balsamo, S.A.; D'Urso, L.; Sciré, S.; Brundo, M.V.; Pecoraro, R.; Scalisi, E.M.; Privitera, V.; Impellizzeri, G. CeO_2 for Water Remediation: Comparison of Various Advanced Oxidation Processes. *Catalysts* **2020**, *10*, 446. [CrossRef]
29. Wang, T.; Wang, Z.; Tang, Y. An integration of photo-Fenton and membrane process for water treatment by a PVDF@$CuFe_2O_4$ catalytic membrane. *J. Membr. Sci.* **2019**, *572*, 419–427. [CrossRef]
30. Arshad, A.; Iqbal, J.; Mansoor, Q. Graphene/Fe_3O_4 nanocomposite: Solar light driven Fenton like reaction for decontamination of water and inhibition of bacterial growth. *Appl. Surf. Sci.* **2019**, *474*, 57–65. [CrossRef]

31. Hassan, A.K.; Rahman, M.M.; Naidu, R. Kinetic of the degradation of sulfanilic acid azochromotrop (SPADNS) by Fenton process coupled with ultrasonic irradiation or L-cysteine acceleration. *Environ. Technol. Innov.* **2019**, *15*, 100380. [CrossRef]
32. Ma, L.; Duan, J.; Yang, Z. Ligand-metal charge transfer mechanism enhances TiO_2/Bi2WO_6/rGO nanomaterials photocatalytic efficient degradation of norfloxacin under visible light. *J. Alloys Compd.* **2021**, *869*, 158679. [CrossRef]
33. Guo, F.; Huang, X.; Shi, W. Investigation of visible-light-driven photocatalytic tetracycline degradation via carbon dots modified porous $ZnSnO_3$ cubes: Mechanism and degradation pathway. *Sep. Purif. Technol.* **2020**, *253*, 117518. [CrossRef]
34. Zhang, Y.; Zhang, Y.; Wang, M. Enhanced photocatalytic reaction and mechanism for treating cyanide-containing wastewater by silicon-based nano-titania. *Hydrometallurgy* **2020**, *198*, 105512. [CrossRef]
35. Mouchaal, Y.; Enesca, A.; Mihoreanu, C.; Khelil, A.; Duta, A. Tuning the opto-electrical properties of SnO2 thin films by Ag^{+1} and In^{+3} co-doping. *Mater. Sci. Eng. B Adv.* **2015**, *199*, 22–29. [CrossRef]
36. Gu, Z.; Cui, Z.; Yin, S. Intrinsic carbon-doping induced synthesis of oxygen vacancies-mediated TiO_2 nanocrystals: Enhanced photocatalytic NO removal performance and mechanism. *J. Catal.* **2021**, *393*, 179–189. [CrossRef]
37. Hwang, J.Y.; Moon, G.; Choi, W. Crystal phase-dependent generation of mobile OH radicals on TiO_2: Revisiting the photocatalytic oxidation mechanism of anatase and rutile. *App. Catal. B* **2021**, *286*, 119905. [CrossRef]
38. Chen, J.; Zhang, Z.; An, T. Superoxide radical enhanced photocatalytic performance of styrene alters its degradation mechanism and intermediate health risk on TiO_2/graphene surface. *Environ. Res.* **2021**, *195*, 110747. [CrossRef]
39. Yang, Y.; Zheng, Y.; Zhang, X. In-situ fabrication of a spherical-shaped Zn-Al hydrotalcite with BiOCl and study on its enhanced photocatalytic mechanism for perfluorooctanoic acid removal performed with a response surface methodology. *J. Hazard. Mater.* **2020**, *399*, 123070. [CrossRef]
40. Zhang, Y.; Zhang, Y.; Wang, M. Adsorptive-photocatalytic performance and mechanism of Me (Mn, Fe)-N co-doped TiO_2/SiO_2 in cyanide wastewater. *J. Alloy. Compd.* **2021**, *867*, 159020. [CrossRef]
41. Fan, G.; Ning, R.; Zhang, J. Double photoelectron-transfer mechanism in Ag−AgCl/WO_3/g-C_3N_4 photocatalyst with enhanced visible-light photocatalytic activity for trimethoprim degradation. *J. Hazard. Mater.* **2021**, *403*, 123964. [CrossRef] [PubMed]
42. Qiao, D.; Li, Z.; He, X. Adsorption and photocatalytic degradation mechanism of magnetic graphene oxide/ZnO nanocomposites for tetracycline contaminants. *Chem. Eng. J.* **2020**, *400*, 125952. [CrossRef]
43. Baneto, M.; Enesca, A.; Mihoreanu, C.; Lare, Y.; Jondo, K.; Napo, K.; Duta, A. Effects of the growth temperature on the properties of spray deposited $CuInS_2$ thin films for photovoltaic applications. *Ceram. Int.* **2015**, *41*, 4742–4749. [CrossRef]
44. Teixeira, G.F.; Silva Junior, E.; Vilela, R.; Zaghete, M.A.; Colmati, F. Perovskite Structure Associated with Precious Metals: Influence on Heterogenous Catalytic Process. *Catalysts* **2019**, *9*, 721. [CrossRef]
45. Wang, Y.F.; Huang, C.X.; Zhu, Y.T. Heterostructure induced dispersive shear bands in heterostructured Cu. *Scripta Mater.* **2019**, *170*, 76–80. [CrossRef]
46. Abdullah, N.R.; Tang, C.-S.; Manolescu, A.; Gudmundsson, V. Manifestation of the Purcell Effect in Current Transport through a Dot–Cavity–QED System. *Nanomaterials* **2019**, *9*, 1023. [CrossRef] [PubMed]
47. Albornoz, L.L.; da Silva, S.W.; Bernardes, A.M. Degradation and mineralization of erythromycin by heterogeneous photocatalysis using SnO_2-doped TiO_2 structured catalysts: Activity and stability. *Chemosphere* **2021**, *268*, 128858. [CrossRef]
48. Das, A.; Patra, M.; Nair, R.G. Role of type II heterojunction in ZnO–In_2O_3 nanodiscs for enhanced visible-light photocatalysis through the synergy of effective charge carrier separation and charge transport. Mater. *Chem. Phys.* **2021**, *263*, 124431.
49. Feng, X.; Yu, Z.; Li, X. 3D MXene/Ag_2S material as Schottky junction catalyst with stable and enhanced photocatalytic activity and photocorrosion resistance. *Sep. Purif. Technol.* **2021**, *266*, 118606. [CrossRef]
50. Li, X.; Jin, Y.; Bao, N. Rational design of *Z*-scheme $Bi_{12}O_{17}Cl_2$/plasmonic Ag/anoxic TiO_2 composites for efficient visible light photocatalysis. *Powder Technol.* **2021**, *384*, 342–352. [CrossRef]
51. Wageh, S.; Al-Ghamdi, A.A.; Zhangc, P. A new heterojunction in photocatalysis: *S*-scheme heterojunction. *Chin. J. Catal.* **2021**, *42*, 667–669. [CrossRef]
52. Kadi, M.W.; Mohamed, R.M.; Bahnemann, D.W. Soft and hard templates assisted synthesis mesoporous CuO/g-C_3N_4 heterostructures for highly enhanced and accelerated Hg(II) photoreduction under visible light. *J. Colloid Interfac. Sci.* **2020**, *580*, 223–233. [CrossRef]
53. Kaur, N.; Zappa, D.; Comini, E. Branch-like NiO/ZnO heterostructures for VOC sensing. *Sens. Actuators B* **2018**, *262*, 477–485. [CrossRef]
54. Yan, X.; Hu, Q.T.; Gu, Z.G. NiCo layered double hydroxide/hydroxide nanosheet heterostructures for highly efficient electrooxidation of urea. *Int. J. Hydrogen Energy* **2020**, *45*, 19206–19213. [CrossRef]
55. Pu, S.; Wang, H.; Zhu, J.; Li, L.; Long, D.; Jian, Y.; Zeng, Y. Heterostructure Cu_2O/(001)TiO_2 Effected on Photocatalytic Degradation of Ammonia of Livestock Houses. *Catalysts* **2019**, *9*, 267. [CrossRef]
56. Bagyalakshmi, B.; Babu, M.; Sundarakannan, B. Temperature-induced strain mediated magnetization changes in $NiFe_2O_4$/$BaTiO_3$ heterostructure. *Ceram. Int.* **2018**, *44*, 15099–15103.
57. Tao, R.; Zhao, C.; Liu, Y. Bi2WO6/$ZnFe_2O_4$ heterostructures nanofibers: Enhanced visible-light photocatalytic activity and magnetically separable property. *Mater. Res. Bull.* **2018**, *104*, 124–133. [CrossRef]
58. Lee, Y.; Kim, S.Y.; Kim, D.Y.; Lee, S. Highly Sensitive UV Photodiode Composed of β-Polyfluorene/YZnO Nanorod Organic-Inorganic Hybrid Heterostructure. *Nanomaterials* **2020**, *10*, 1486. [CrossRef] [PubMed]

59. Enesca, A.; Isac, L.; Duta, A. Charge carriers injection in tandem semiconductors for dyes mineralization. *Appl. Catal. B.* **2015**, *162*, 352–363. [CrossRef]
60. Qin, Y.; Wang, Z.; Wu, K. One-step fabrication of TiO_2/Ti foil annular photoreactor for photocatalytic degradation of formaldehyde. *Chem. Eng. J.* **2020**, *394*, 124917. [CrossRef]
61. Xiong, Z.; Lei, Z.; Wu, J.C.S. Photocatalytic CO_2 reduction over V and W codoped TiO_2 catalyst in an internal-illuminated honeycomb photoreactor under simulated sunlight irradiation. *App. Catal. B* **2017**, *219*, 412–424. [CrossRef]
62. Supplis, C.; Gros, F.; Cornet, J.F. Spectral radiative analysis of bio-inspired H_2 production in a benchmark photoreactor: A first investigation using spatial photonic balance. *Int. J. Hydrogen Energy* **2018**, *43*, 8221–8231. [CrossRef]
63. Sawicka, M.J.; Lubkowski, K.; Soroka, J.A. Synthesis of 7H-indolo[1,2-a]quinolinium derivatives via oxidative photocyclization of 3H-indolium salts using blue LED photoreactor. *Tetrahedron* **2019**, *75*, 3822–3831. [CrossRef]
64. Neolaka, Y.A.B.; Ngara, Z.S.; Kusuma, H.S. Simple design and preliminary evaluation of continuous submerged solid small-scale laboratory photoreactor (CS4PR) using TiO_2/NO_3-@TC for dye degradation. *J. Environ. Chem. Eng.* **2019**, *7*, 103482. [CrossRef]
65. Manjunath, S.V.; Tripathy, B.K.; Pramod, S. Simultaneous degradation of anionic and cationic dyes from multi-dye systems using falling film photoreactor: Performance evaluation, kinetic and toxicity analysis. *J. Environ. Chem. Eng.* **2020**, *8*, 104486.
66. Azam, M.U.; Tahir, M.; Nawawi, M.G.M. Engineering approach to enhance photocatalytic water splitting for dynamic H_2 production using La_2O_3/TiO_2 nanocatalyst in a monolith photoreactor. *App. Surf. Sci.* **2019**, *484*, 1089–1101. [CrossRef]
67. Tasleem, S.; Tahir, M. Investigating the performance of liquid and gas phase photoreactors for dynamic H_2 production over bimetallic TiO_2 and $N_{i2}P$ dispersed MAX Ti_3AlC_2 monolithic nanocomposite under UV and visible light. *J. Environ. Chem. Eng.* **2021**, *9*, 105351. [CrossRef]
68. Kumaravel, V.; Imam, M.D.; Badreldin, A.; Chava, R.K.; Do, J.Y.; Kang, M.; Abdel-Wahab, A. Photocatalytic Hydrogen Production: Role of Sacrificial Reagents on the Activity of Oxide, Carbon, and Sulfide Catalysts. *Catalysts* **2019**, *9*, 276. [CrossRef]
69. Abdel-Maksoud, Y.K.; Imam, E.; Ramadan, A.R. TiO_2 water-bell photoreactor for wastewater treatment. *Solar Energy* **2018**, *170*, 323–335. [CrossRef]
70. Mirzaei, M.; Jafarikojour, M.; Dabir, B.; Dadvar, M. Evaluation and modeling of a spinning disc photoreactor for degradation of phenol: Impact of geometry modification. *J. Photochem. Photobiol. A* **2017**, *346*, 206–214. [CrossRef]
71. Najafabadi, S.M.; Rashidi, F.; Rezaei, M. Performance of a multistage rotating mesh support photoreactor immobilized with TiO_2 on photocatalytic degradation of PNP: Reactor construction and optimization. *Chem. Eng. Process. Process Intensif.* **2019**, *146*, 107668. [CrossRef]
72. Palmisano, G.; Loddo, V.; Augugliaro, V.; Bellardita, M.; Roda, G.C.; Parrino, F. Validation of a two-dimensional modeling of an externally irradiated slurry photoreactor. *Chem. Eng. J.* **2015**, *262*, 490–498. [CrossRef]
73. Zheng, Q.; Aiello, A.; Choi, Y.S.; Tarr, K.; Shen, H.; Durkin, D.P.; Shuai, D. 3D printed photoreactor with immobilized graphitic carbon nitride: A sustainable platform for solar water purification. *J. Hazard. Mater.* **2020**, *399*, 123097. [CrossRef]
74. Espíndola, J.C.; Cristóvão, R.O.; Mayer, D.A.; Boaventura, R.A.R.; Dias, M.M.; Lopes, J.C.B.; Vilar, V.J.P. Overcoming limitations in photochemical UVC/H_2O_2 systems using a mili-photoreactor (NETmix): Oxytetracycline oxidation. *Sci. Total Environ.* **2019**, *660*, 982–992. [CrossRef]
75. Lin, C.C.; Wu, M.S. Feasibility of using UV/H_2O_2 process to degrade sulfamethazine in aqueous solutions in a large photoreactor. *J. Photochem. Photobiol. A* **2018**, *367*, 446–451. [CrossRef]
76. Russo, D.; Spasiano, D.; Vaccaro, M.; Andreozzi, R.; Li Puma, G.; Reis, N.M.; Marotta, R. Direct photolysis of benzoylecgonine under UV irradiation at 254 nm in a continuous flow microcapillary array photoreactor. *Chem. Eng. J.* **2016**, *283*, 243–250. [CrossRef]
77. Moussavi, G.; Momeninejad, H.; Shekoohiyan, S.; Baratpour, P. Oxidation of acetaminophen in the contaminated water using UVC/S_2O_8-2 process in a cylindrical photoreactor: Efficiency and kinetics of degradation and mineralization. *Sep. Purif. Technol.* **2017**, *181*, 132–138. [CrossRef]
78. Karimian, S.; Moussavi, G.; Fanaei, F.; Mohammadi, S.; Shekoohiyan, S.; Giannakis, S. Shedding light on the catalytic synergies between Fe(II) and PMS in vacuum UV (VUV/Fe/PMS) photoreactors for accelerated elimination of pharmaceuticals: The case of metformin. *Chem. Eng. J.* **2020**, *400*, 125896. [CrossRef]
79. Vaiano, V.; Matarangolo, M.; Sacco, O. UV-LEDs floating-bed photoreactor for the removal of caffeine and paracetamol using ZnO supported on polystyrene pellets. *Chem. Eng. J.* **2018**, *350*, 703–713. [CrossRef]
80. Ochoa-Gutiérrez, K.S.; Tabares-Aguilar, E.; Mueses, M.A.; Machuca-Martínez, F.; Li Puma, G. A Novel Prototype Offset Multi Tubular Photoreactor (OMTP) for solar photocatalytic degradation of water contaminants. *Chem. Eng. J.* **2018**, *341*, 628–638. [CrossRef]
81. Diaz-Angulo, J.; Arce-Sarria, A.; Mueses, M.; Hernandez-Ramirez, A.; Machuca-Martinez, F. Analysis of two dye-sensitized methods for improving the sunlight absorption of TiO_2 using CPC photoreactor at pilot scale. *Mater. Sci. Semicond. Process.* **2019**, *103*, 104640. [CrossRef]
82. Alahiane, S.; Sennaoui, A.; Sakr, F.; Dinne, M.; Qourzal, S.; Assabbane, A. Synchronous role of coupled adsorption-photocatalytic degradation of Direct Red 80 with nanocrystalline TiO_2-coated non-woven fibres materials in a static batch photoreactor. *Groundw. Sustain. Dev.* **2020**, *11*, 100396. [CrossRef]
83. Lin, C.C.; Sun, C.C. Decolorization of high-concentration Reactive Red 2 in water using UV and persulfate in a 3-liter photoreactor. *J. Taiwan Inst. Chem. Eng.* **2020**, *115*, 169–174. [CrossRef]

84. Mesgari, Z.; Saien, J. Pollutant degradation over dye sensitized nitrogen doped titania substances in different configurations of visible light helical flow photoreactor. *Sep. Purif. Technol.* **2017**, *185*, 129–139. [CrossRef]
85. Li, D.; Zheng, H.; Wang, Q.; Wang, X.; Jiang, W.; Zhang, Z.; Yang, Y. A novel double-cylindrical-shell photoreactor immobilized with monolayer TiO2-coated silica gel beads for photocatalytic degradation of Rhodamine B and Methyl Orange in aqueous solution. *Sep. Purif. Technol.* **2014**, *123*, 130–138. [CrossRef]
86. Santoro, D.; Crapulli, F.; Turolla, A.; Antonelli, M. Detailed modeling of oxalic acid degradation by UV-TiO_2 nanoparticles: Importance of light scattering and photoreactor scale-up. *Water Res.* **2017**, *121*, 361–373. [CrossRef]
87. Rahmani, E.; Rahmani, M.; Silab, H. TiO_2:SiO_2 thin film coated annular photoreactor for degradation of oily contamination from waste water. *J. Water Process. Eng.* **2020**, *37*, 101374. [CrossRef]
88. Ghafoori, S.; Mehrvar, M.; Chan, P.K. Photoreactor scale-up for degradation of aqueous poly(vinyl alcohol) using UV/H_2O_2 process. *Chem. Eng. J.* **2014**, *245*, 133–142. [CrossRef]
89. Vaiano, V.; Sacco, O.; Pisano, D.; Sannino, D.; Ciambelli, P. From the design to the development of a continuous fixed bed photoreactor for photocatalytic degradation of organic pollutants in wastewater. *Chem. Eng. Sci.* **2015**, *137*, 152–160. [CrossRef]
90. Di Capua, G.; Femia, N.; Migliaro, M.; Sacco, O.; Sannino, D.; Stoyka, K.; Vaiano, V. Intensification of aflat-plate photocatalytic reactor performances byinnovative visible light modulation techniques: A proof of concept. *Chem. Eng. Process. Process Intensif.* **2017**, *118*, 117–123. [CrossRef]
91. Sutisna; Rokhmat, M.; Wibowo, E.; Khairurrijal; Abdullah, M. Prototype of a flat-panel photoreactor using TiO_2 nanoparticles coated on transparent granules for the degradation of Methylene Blue under solar illumination. *Sustain. Environ. Res.* **2017**, *27*, 172–180.
92. Sutisna; Rokhmat, M.; Wibowo, E.; Murniati, R.; Khairurrijal; Abdullah, M. Novel Solar Photocatalytic Reactor for Wastewater Treatment. *IOP Conf. Ser. Mater. Sci. Eng.* **2017**, *214*, 012010.
93. Zhang, C.; Sabouni, R.; Shao, Y.; Goma, H.G. Performance of submerged oscillatory membrane photoreactor for water treatment. *J. Environ. Chem. Eng.* **2017**, *5*, 3330–3336. [CrossRef]
94. Bukman, L.; de Freitas, C.F.; Caetano, W.; Fernandes, N.R.C.; Hioka, N.; Batistela, V.R. Kinetic spectrophotometric method for real-time monitoring of ultraviolet photoreactions: A mini-photoreactor. *Spectrochim. Acta A* **2019**, *211*, 330–335. [CrossRef]
95. Grcic, I.; Li Puma, G. Six-flux absorption-scattering models for photocatalysis underwide-spectrum irradiation sources in annular and flat reactors usingcatalysts with different optical properties. *App. Catal. B* **2017**, *211*, 222–234. [CrossRef]
96. Wang, P.; Lim, T.T. Membrane vis-LED photoreactor for simultaneous penicillin G degradation and TiO_2 separation. *Water Res.* **2012**, *46*, 1825–1837. [CrossRef]
97. Almansba, A.; Kane, A.; Nasrallah, N.; Maachi, R.; Lamaa, L.; Peruchon, L.; Brochier, C.; Bechohra, I.; Amrane, A.; Assadi, A.A. Innovative photocatalytic luminous textiles optimized towards water treatment: Performance evaluation of photoreactors. *Chem. Eng. J.* **2021**, *416*, 129195. [CrossRef]
98. Roselin, L.S.; Rajarajeswari, G.R.; Selvin, R.; Sadasivam, V.; Sivasankar, B.; Rengaraj, K. Sunlight/ZnO-mediated photocatalytic degradation of reactive red 22 using thin film flat bed flow photoreactor. *Sol. Energy* **2002**, *73*, 281–285. [CrossRef]
99. Aoudjit, L.; Martins, P.M.; Madjene, F.; Petrovykh, D.Y.; Lanceros-Mendez, S. Photocatalytic reusable membranes for the effective degradation of tartrazine with a solar photoreactor. *J. Hazard. Mater.* **2018**, *344*, 408–416. [CrossRef]
100. Foulady-Dehaghi, R.; Behpour, M. Visible and solar photodegradation of textile wastewater by multiple doped TiO_2/Zn nanostructured thin films in fixed bed photoreactor mode. *Inorg. Chem. Commun.* **2020**, *117*, 107946. [CrossRef]
101. Kassahun, S.K.; Kiflie, Z.; Kim, H.; Gadisa, B.T. Effects of operational parameters on bacterial inactivation in Vis-LEDs illuminated N-doped TiO2 based photoreactor. *J. Environ. Chem. Eng.* **2020**, *8*, 104374. [CrossRef]
102. Azadi, S.; Karimi-Jashni, A.; Javadpour, S.; Amiri, H. Photocatalytic treatment of landfill leachate using cascade photoreactor with immobilized W-C-codoped TiO_2 nanoparticles. *J. Water Proc. Eng.* **2020**, *36*, 101307. [CrossRef]
103. Joven-Quintero, S.A.; Castilla-Acevedo, S.F.; Betancourt-Buitrago, L.A.; Acosta-Herazo, R.; Machuca-Martinez, F. Photocatalytic degradation of cobalt cyanocomplexes in a novel LED photoreactor using TiO_2 supported on borosilicate sheets: A new perspective for mining wastewater treatment. *Mater. Sci. Semicond. Proc.* **2020**, *110*, 104972. [CrossRef]
104. Devia-Orjuel, J.S.; Betancourt-Buitrago, L.A.; Machuca-Martinez, F. CFD modeling of a UV-A LED baffled flat-plate photoreactor for environment applications: A mining wastewater case. *Environ. Sci. Pollut. Res.* **2020**, *26*, 4510–4520. [CrossRef]
105. Bahmani, M.; Dashtian, K.; Mowla, D.; Esmaeilzadeh, F.; Ghaedi, M. UiO-66(Ti)-Fe_3O_4-WO_3 photocatalyst for efficient ammonia degradation from wastewater into continuous flow-loop thin film slurry flat-plate photoreactor. *J. Hazard. Mater.* **2020**, *393*, 122360. [CrossRef] [PubMed]
106. Larijani, R.S.; Ghadiri, M.; Hafezi, M.; Jafarikojour, M.; Dabir, B. Evaluation of mass and photon transfer enhancement by an impinging jet atomization photoreactor for photocatalytic degradation of p-nitrophenol. *J. Photochem. Photobiol. A* **2021**, *408*, 113088. [CrossRef]
107. Kim, S.; Cho, H.; Joo, H.; Her, N.; Han, J.; Yi, K.; Kim, J.O.; Yoon, J. Evaluation of performance with small and scale-up rotating and flatreactors; photocatalytic degradation of bisphenol A, 17 β-estradiol, and 17 α-ethynyl estradiol under solar irradiation. *J. Hazard. Mater.* **2017**, *336*, 21–32. [CrossRef]